CONTROL OF NTMS AND INTEGRATED MULTI-ACTUATOR CONTROL ON TCV

M. KONG[1], T.C. BLANKEN[2], F. CARPANESE[1], F. FELICI[1], C. GALPERTI[1], E. MALJAARS[2], A. MERLE[1], J-M. MORET[1], F. PESAMOSCA[1], E. POLI[3], M. REICH[3], O. SAUTER[1], A.A. TEPLUKHINA[1], T. VU[1], the TCV team* and the EUROfusion MST1 Team†

[1] École Polytechnique Fédérale de Lausanne (EPFL), Swiss Plasma Center (SPC)
Lausanne, Switzerland
[2] Eindhoven University of Technology, Department of Mechanical Engineering
Eindhoven, the Netherlands
[3] Max-Planck Institut für Plasmaphysik
Garching, Germany

Email: mengdi.kong@epfl.ch

Abstract

The control of neoclassical tearing modes (NTMs) located at the m=2/n=1 rational surface (where m and n are the poloidal and toroidal mode number respectively) with electron cyclotron (EC) waves has been studied both experimentally and numerically on TCV. A small sinusoidal sweeping has been added to the control beam and is proven for the first time to be effective for both stabilizing and preempting 2/1 NTMs. It is also shown that preemption is more than twice as efficient as stabilization in terms of the minimum power required, at least when sweeping is applied. Based on the tearing mode triggered nature of these 2/1 NTMs, a simple analytical model has been proposed to evaluate the time-varying classical stability index Δ', which allows one to simulate very well the entire island width evolution, starting from zero width for the first time. The reliable and efficient control of NTMs has facilitated the development of a NTM controller that is independent of the special features of TCV and has been included in a newly built generic plasma control system (PCS). Simultaneous control of 2/1 NTMs and plasma β (the ratio of plasma pressure to magnetic pressure) has been successfully demonstrated on TCV with this new PCS, including generic real-time (RT) plasma state reconstruction, monitoring, controllers, and advanced supervisory controller and actuator manager (AM).

1. INTRODUCTION

Neoclassical tearing modes (NTMs) located at the m=2/n=1 rational surface (where m and n are the poloidal and toroidal mode number respectively) can cause a more than 20% confinement degradation, decrease the Q factor (ratio between the fusion and auxiliary heating powers) and frequently lead to plasma disruptions, especially in high confinement mode (H-mode) plasmas [1][2]. This is beyond the acceptable level for ITER, highlighting the importance of better understanding the physics of NTMs and of their reliable control. Given the localization of its deposition, the electron cyclotron (EC) wave has proven to be promising in the effective control of NTMs and will be used in ITER [3]. The effect of EC beams on the stability and control of NTMs is twofold: by modifying the current density profile and thus the stability index of the TM (Δ'), and by replacing the missing bootstrap current within the magnetic island through direct current drive (ECCD) or indirect heating effect (ECH) [3]. Much theoretical work has been performed to clarify the effects of various driving terms on the evolution of the island width, either with the Modified Rutherford Equation (MRE) [1]-[4][and references therein] or the MHD model [5][and references therein]. Meanwhile, experimental studies concerning the stabilization and preemption of NTMs have been performed on several tokamaks, mostly about 3/2 NTMs and a few on 2/1 NTMs [1][6]-[9][and references therein]. Although similar physics is involved in 3/2 and 2/1 NTMs, the control of 2/1 NTMs is more challenging due to their typically stronger growth rate and proximity to the plasma edge, which on one hand increases the chance of mode locking and disruptions and on the other hand decreases the ECCD efficiency. The efficient and reliable control of 2/1 NTMs is thus a major concern for ITER and needs to be ensured. In this respect, more experimental efforts are still needed to carefully isolate the different effects, emphasize the (range of) validity of theoretical models and improve the control algorithms.

In this paper, dedicated experiments on the control of 2/1 NTMs on TCV and interpretative modeling with the MRE are presented. With the relatively short time scale of TCV (confinement time ~ 5ms and resistive ~ 100ms) and its flexible EC system, different plasma conditions and various aspects of NTM control have been explored. For instance, a small sinusoidal sweeping of the radial deposition location of the EC power has been added to the control beam and is proven to be effective for both stabilizing and preempting 2/1 NTMs for the first time. The inclusion of the small sweeping allows one to develop a reliable NTM controller irrespective of the plasma

* See the author list of S. Coda et al., 2017 Nucl. Fusion 57 102011

† See the author list of H. Meyer et al., 2017 Nucl. Fusion 57 102014

scenarios since it reduces the difficulties caused by the inaccuracies of the equilibrium reconstruction that may vary with different plasma scenarios. A generic controller is thus developed and has been included in an integrated control scheme, which will be discussed in the second part of this paper. It is also shown that preemption is more than twice as efficient as stabilization in terms of the minimum power required, at least when sweeping is applied. Based on the anticipated Δ' triggered nature of the 2/1 NTMs involved on TCV, a simple analytical model is proposed to evaluate the time-varying Δ', which for the first time allows the simulation of the entire island width evolution, starting from zero width.

The reliable and generic NTM controller can be readily integrated with other real-time (RT) algorithms needed for tokamak operation. For large devices like ITER, supervising the plasma discharge evolution and performing multiple control tasks sharing a limited set of actuators is especially important [7]. This requires reliable RT plasma state reconstruction, monitoring and supervision, an actuator manager (AM) and controllers. Following a generic integrated control framework, all the above mentioned components have been implemented and tested experimentally on TCV. Simultaneous control of NTMs, β (the ratio of plasma pressure to magnetic pressure) and model-estimated safety factor (q) profiles has been achieved with this system [10]-[15].

2. NTM PHYSICS AND CONTROL

2.1 Plasma scenario and experimental setup

In the NTM experiments, limited L-mode plasmas with constant plasma current ($I_p \approx 110kA$) and magnetic field ($B_0 \approx 1.44T$) are used. A central line-averaged density of $n_{el} \approx 1.8 \times 10^{19} m^{-3}$ is kept to ensure 100% absorption of EC waves. Two second harmonic X-mode (X2) EC gyrotrons with a nominal power of 0.5MW each are used to drive on-axis current in the same direction as I_p (i.e. co-ECCD), through two independent launchers with steerable mirrors. 2/1 NTMs are destabilized through the modification of the current density profile with this central co-ECCD, i.e. a Δ' effect [11]. The mode then grows neoclassically with the effect of perturbed bootstrap current. A third X2 gyrotron with a nominal power of 0.75MW and an independent launcher is used for control purposes. The toroidal angles of these launchers are set before the experiment to allow for co-ECCD, counter-CD or ECH, while their poloidal angles can be RT controlled by feedforward or feedback commands to vary the deposition location of the EC beams.

2.2 Theoretical model

The MRE model is used to quantify the effect of different terms on the overall evolution of the island width w, and can be written as [3][16][17]:

$$\frac{\tau_R}{\overline{\rho}_{mn}}\frac{dw}{dt} = \overline{\rho}_{mn}\Delta' + \overline{\rho}_{mn}\Delta'_{BS} + \overline{\rho}_{mn}\Delta'_{GGJ} + \overline{\rho}_{mn}\Delta'_{CD} + \overline{\rho}_{mn}\Delta'_{H}, \tag{2.1}$$

with

$$\overline{\rho}_{mn}\Delta'_{BS} = a_2\overline{\rho}_{mn}\beta_p\left|L_{bs}\right|\frac{L_q}{(-L_p)}\frac{w}{w^2+w_{de}^2} = a_2\overline{\rho}_{mn}\frac{2\mu_0 R_0 q_{mn}}{s_{mn}B_0}j_{bs,mn}\frac{w}{w^2+w_{de}^2}, \tag{2.2}$$

$$\overline{\rho}_{mn}\Delta'_{GGJ} = -a_3\overline{\rho}_{mn}\frac{6D_R}{\sqrt{w^2+0.2w_{de}^2}} = -\frac{12\mu_0 R_0^2}{B_0^2}\frac{\epsilon_{mn}^2}{s_{mn}^2}\frac{p_{mn}}{(-L_p)}\frac{(q_{mn}^2-1)}{\sqrt{w^2+0.2w_{de}^2}}, \tag{2.3}$$

$$\overline{\rho}_{mn}\Delta'_{CD} = -a_4\frac{16\mu_0 R_0 q_{mn}}{\pi s_{mn}B_0}\frac{I_{cd}}{w_{dep}^2}N_{cd}(\frac{w}{w_{dep}})G_{cd}(\frac{w}{w_{dep}},\overline{\rho}_{dep})M_{cd}(\frac{w}{w_{dep}},D), \tag{2.4}$$

and

$$\overline{\rho}_{mn}\Delta'_{H} = -a_5\frac{16\mu_0 R_0 q_{mn}}{\pi s_{mn}B_0}\frac{\eta_H P_{abs}}{w_{dep}^2}N_H(\frac{w}{w_{dep}})G_H(\frac{w}{w_{dep}},\overline{\rho}_{dep})M_H(\frac{w}{w_{dep}},D), \tag{2.5}$$

where the subscript "mn" represents the value evaluated at the $q = m/n$ rational surface; $\overline{\rho}$ is the radial location of flux surfaces defined by $\overline{\rho} = \sqrt{\frac{\Phi}{\pi B_0}} \cdot a$, with Φ the toroidal flux contained by a given flux surface and a the minor radius; $\tau_R = \frac{\mu_0 \overline{\rho}_{mn}^2}{1.22\eta_{neo}}$ is the effective resistive time and η_{neo} the neoclassical resistivity at the rational surface [18]; a_2 to a_5 are the "free" parameters to account for the assumptions in the model and the uncertainties in the data to fit the experimental results, where a_2, for example, was taken as 2.6 to match the observed saturated island width when assuming $\overline{\rho}_{mn}\Delta' = -m$ [16]; β_p is the ratio of plasma pressure p to poloidal magnetic pressure $\frac{B_p^2}{2\mu_0}$, and has been replaced by $\beta_p = \frac{2\mu_0 p}{B_p^2} \approx \frac{2\mu_0 p_{mn} R_0^2 q_{mn}^2}{\overline{\rho}_{mn}^2 B_0^2}$ through the approximate relation between B_p and B_0; $L_q = \frac{q}{dq/d\overline{\rho}} = \overline{\rho}s$, where s is the magnetic shear; $L_p = \frac{p}{dp/d\overline{\rho}}$; $\epsilon = a/R_0$, where R_0 is the major radius (0.88m for TCV); $D_R = \frac{\epsilon^2\beta_p}{s}\frac{L_q}{-L_p}(1-\frac{1}{q^2})$; w_{de} accounts for the finite ratio of perpendicular to parallel heat transport $\chi_\perp/\chi_\parallel$ at small w [19] and is given by $w_{de} = \left[5.1(\frac{1}{\epsilon sn})^{\frac{1}{2}}\right]^{\frac{4}{3}}(\frac{\chi_\perp}{\chi_\parallel})^{\frac{1}{3}}\overline{\rho}_{mn}$ [1]; I_{cd} is the total driven current from a given EC launcher, P_{abs} the absorbed power, $\overline{\rho}_{dep}$ the location of the peak of the deposited power density and w_{dep} the full e^{-1} width; η_H estimates the efficiency with which the EC power is

converted into a perturbative inductive current and is given by [17] $\eta_H = \frac{3w_{dep}^2}{8\pi R n_{e,mn}\chi_\perp k_B}\frac{j_{sep}}{T_{sep}}$, where $n_{e,mn}$ refers to the local electron density, k_B is the Boltzmann constant, j_{sep} refers to the inductive part of the current density at the island separatrix and T_{sep} is the corresponding electron temperature; the N, G and M terms in Eqs. (2.4) and (2.5) represent the dependence on w, the misalignment with respect to the $q = m/n$ surface and the effect of modulation, respectively, following the definitions in [17]; D is the power on-time fraction and equals 1 for the continuous wave injection used in the tests here.

The classical stability index $\overline{\rho}_{mn}\Delta'$ can be in principle calculated from the equilibrium and effective *q* profile, but is very sensitive to the derivatives of *q* and hard to evaluate well. For simulations with MRE, a typical approach is to use a medium value between marginal classical stability $\overline{\rho}_{mn}\Delta' = 0$ and strong stability $\overline{\rho}_{mn}\Delta' = -2m$ [1]-[3], thus $\overline{\rho}_{mn}\Delta' = -m$ assuming w is relatively large. As the saturated island width (w_{sat}) without EC (i.e. $\Delta'_{CD} = \Delta'_H = 0$) is dominated by Δ'_{BS}/Δ', a different value of $\overline{\rho}_{mn}\Delta'$ would require a different coefficient a_2 to fit the experimental w. For NTMs that are triggered by unstable q profiles (i.e. positive Δ' at $w = 0$), as the ones here, the stabilizing effect of the modification of the current density by the island itself needs to be considered [20][21] to simulate the full time evolution:

$$\overline{\rho}_{mn}\Delta' = \overline{\rho}_{mn}\Delta'_0 - \alpha\frac{w}{\overline{\rho}_{mn}}, \tag{2.6}$$

where $\overline{\rho}_{mn}\Delta'_0$ represents the stability at $w = 0$ and is positive at the time of triggering, and a first approximation of α can be given by taking the lowest order terms from [21]:

$$\alpha \approx \frac{m^2a^2}{\overline{\rho}_{mn}^2}(1 - \frac{s\overline{\rho}_{mn}}{ma}), \tag{2.7}$$

while ensuring $\alpha > 0$ by taking for example the maximum between Eq. (2.7) and m. It is possible to measure α through dedicated experiments. For example [20] gives $\alpha = \alpha_{Ref[20]} \cdot \overline{\rho}_{mn} \approx 33[m^{-1}] \cdot 0.12[m] \approx 4$ in similar plasmas as used here. However, quasilinear effects resulting from the flattening of the current profile as the island develops have been found to be important [22], and we define here an ad-hoc model both considering these quasilinear effects and representing a stationary $\overline{\rho}_{mn}\Delta'$ value for large w, consistent with previous simulations [2][3][16]:

$$\overline{\rho}_{mn}\Delta' = \overline{\rho}_{mn}\Delta'_0 - \frac{(\overline{\rho}_{mn}\Delta'_0 + \overline{\rho}_{mn}\Delta'_{sat})w}{\sqrt{w^2 + ((\overline{\rho}_{mn}\Delta'_0 + \overline{\rho}_{mn}\Delta'_{sat})\overline{\rho}_{mn}/\alpha)^2}}, \tag{2.8}$$

where $\overline{\rho}_{mn}\Delta'_{sat}$ represents the value at large w. In this case, Eq. (2.8) gives $\overline{\rho}_{mn}\Delta' = \overline{\rho}_{mn}\Delta'_{sat}$ for relatively large w and recovers Eq. (2.6) at small w.

2.3 Experimental and simulation results

2.3.1 Slow ramp down of central co-ECCD power

As shown in Fig. 1, 0.9MW of X2 EC power in total is turned on at 0.4s and deposits co-ECCD at the plasma center through two launchers (L_4 and L_6). A 2/1 NTM is triggered at about 0.5s, 100ms (i.e. the current redistribution time) after switching on the EC power and is sustained. Starting from 1.2s, the EC power is slowly ramped down and reaches a total power of about 0.35MW at 2.1s when the mode self-stabilizes.

To quantify the effects of various terms on the island width evolution, simulations with the MRE model (Eq. (2.1) -Eq. (2.9)) have been performed. Following the discussions in Section 2.2, Eq. (2.8) is used here to allow for simulating the entire island width evolution, starting from $w = 0$, while $\overline{\rho}_{mn}\Delta'_0$ and $\overline{\rho}_{mn}\Delta'_{sat}$ still need to be specified. Given the q-profile triggered nature of these modes (through central co-ECCD deposition), I_{cd} is expected to play a role in $\overline{\rho}_{mn}\Delta'_0$ and a simple analytical model is proposed:

$$\overline{\rho}_{mn}\Delta'_0 = \overline{\rho}_{mn}\Delta'_{ohmic0} + k_{cd}\frac{I_{cd}}{I_p}, \tag{2.9}$$

where $\overline{\rho}_{mn}\Delta'_{ohmic0}$ refers to the stability index in case of no EC power (i.e. ohmic) and zero island width, and $k_{cd}\frac{I_{cd}}{I_p}$ represents the modification of the stability by ECCD. The value of $\overline{\rho}_{mn}\Delta'_{ohmic0}$ is found to be related to density and is estimated through dedicated experiments (e.g., power ramps under various density levels, density ramps, etc.) and simulations, together with the value of k_{cd}. More details concerning this part will be presented in another paper [23]. Interpretative simulations with the transport code ASTRA [24] show that the magnetic shear at the 2/1 surface, s_{21}, increases with increasing central I_{cd} (under constant I_p), which explains Eq. (2.9) to some extent.

Together with other experimental data (e.g., n_e and T_e from Thomson scattering measurements), EC relevant parameters from the ray-tracing code TORAY-GA [25] such as I_{cd}, P_{abs}, $\overline{\rho}_{dep}$ and w_{dep} are used by ASTRA to solve consistently the profiles used in the simulations, e.g., q, s, j_{bs}, etc. Given in Table 1 are the key coefficients used in the simulations. As illustrated in Fig. 2, $\overline{\rho}_{mn}\Delta'_0$ is evaluated based on Eq. (2.9), and is then used by Eq. (2.8) to estimate the time-varying $\overline{\rho}_{mn}\Delta'$. This allows one to simulate the entire w evolution from $w = 0$. As shown in Fig. 3, the simulated island width (red) fits very well the measured width (blue), in terms of the triggering, the w_{sat} and the full stabilization; the green curve represents the β_p trace that dominates the $\overline{\rho}_{mn}\Delta'_{bs}$ term and is scaled based on the w_{ref} (typically w_{sat}) at a selected t_{ref}, i.e. $w_{scaled}(t) = \frac{\beta_P(t)}{\beta_p(t_{ref})} w_{ref}$. The phase plot ($\frac{dw}{dt}$ versus w) at several interesting time slices are shown in Fig. 4, and the dashed magenta curve is taken from the measured island width evolution in the experiment. On can see that at $t = 0.5s$, $\frac{dw}{dt} > 0$ at $w = 0$ (due to a positive $\overline{\rho}_{mn}\Delta'$) and the mode starts to grow, representing the onset of the mode; at $t = 1s$, $\frac{dw}{dt} \approx 0$ at $w_{sat} = 5cm$; from $t = 1.2s$, the EC power is ramped down slowly and $\frac{dw}{dt} \approx 0$ is sustained with decreasing w_{sat}; at $t = 2.1s$, the maximum of $\frac{dw}{dt}$ goes below 0 and the mode is fully stabilized; after turning off the EC power at $t = 2.25s$, the entire $\frac{dw}{dt}$ curve remains negative and the plasma is stable to NTMs.

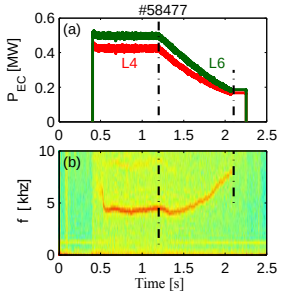

FIG. 1. (a) EC power trace and (b) NTM spectrogram of the slow power ramp down experiment (#58477)

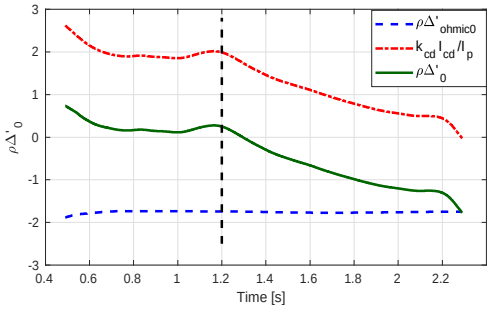

FIG. 2. Time-dependent $\overline{\rho}_{mn}\Delta'_0$ based on Eq. (2.9)

TABLE 1. List of the key coefficients used in the MRE simulations

Shot #	$I_p, [kA]$	$w_{de}, [cm]$	k_{cd}	α	$\overline{\rho}_{mn}\Delta'_{sat}$	a_2	a_3	a_4	a_5
58477	110	1.8	6	5	-1.4	2.1	1	0.2	1.5

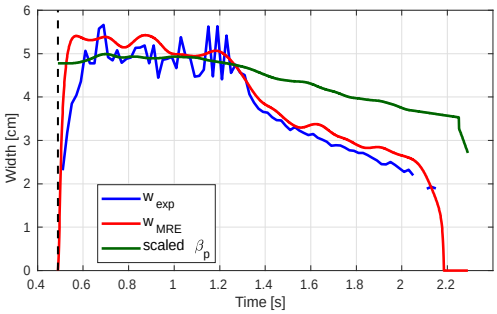

FIG. 3. Full island width evolution (#58477)

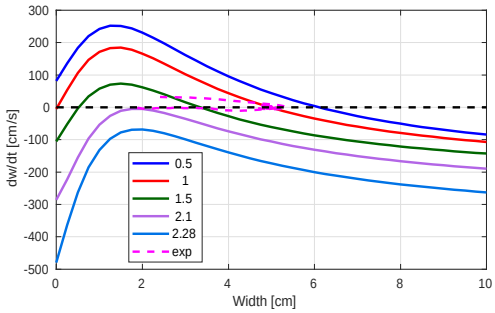

FIG. 4. Phase plot ($\frac{dw}{dt}$ versus w) at several time slices

2.3.2 NTM stabilization test with varying co-ECCD deposition location

In the 2/1 NTM stabilization test shown in Fig. 5, a 3rd co-ECCD launcher ($L1$) with a power of 0.75MW is turned on at 0.8s and moved towards the mode location from 1s to stabilize the mode. L_4 and L_6 remain at the plasma center with a slow ramping down of their power from 0.9s and reach a total power of 0.6MW at $t = 2.25s$. The 2/1 NTM is fully stabilized at $t = 1.25s$ when $L1$ crosses the mode location for the first time. Note that $L1$ then sweeps around the $q = 2$ surface and no mode is destabilized.

Simulations with the MRE model have been done, as shown in Fig. 6. The simulated island width evolution starting from $w = 0$ reproduces very well the measured width. The same coefficients as in the previous example (#58477, Table 1) have been used, except for w_{de} and a_2, where slightly different values are utilized: $w_{de} = 2.2cm$ instead of $1.8cm$ and $a_2 = 1.6$ instead of 2.1. This can be explained by slightly different plasma conditions in these shots. It is worth mentioning that $a_4 = 0.2$ (for Δ'_{CD}) and $a_5 = 1.5$ (for Δ'_H) used in these

simulations are determined by a series of NTM stabilization experiments with $L1$ in either co-ECCD, counter-ECCD or ECH and relevant simulations with the MRE, though not detailed here. Note that the slight ramp down of central co-ECCD power in this case is not able to fully stabilize the mode until around 2s, as indicated by the dashed magenta curve in Fig. 6, where the simulation is performed assuming no $L1$ power is added. This confirms that it is the local ECCD and ECH effect from $L1$ that fully stabilize the mode at $t = 1.25s$. Fig. 7 shows the phase plot at several typical time slices, concerning the triggering ($t = 0.55s$), the $w_{sat} = 3.5cm$ phase ($t = 0.72s$), the $w_{sat} = 5cm$ phase ($t = 0.9s$), the full stabilization ($t = 1.25s$), the phase with EC power but no mode ($t = 2s$) as well as the ohmic phase after turning off the EC power ($t = 2.28s$).

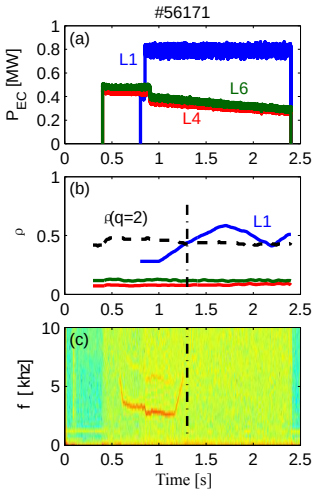

FIG. 5. (a) EC power trace, (b) EC deposition location and (c) magnetic spectrogram of the NTM stabilization experiment (#56171)

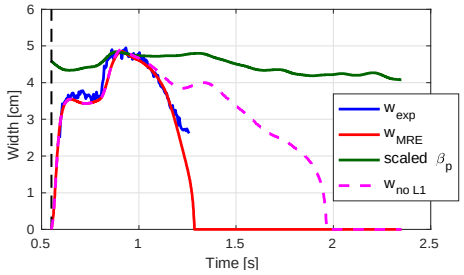

FIG. 6. Full island width evolution (#56171)

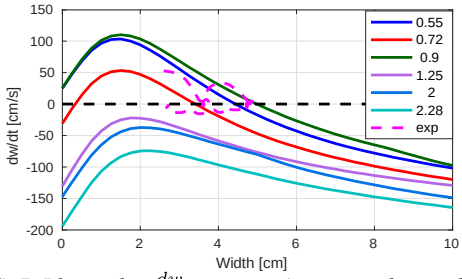

FIG. 7. Phase plot ($\frac{dw}{dt}$ versus w) at several time slices

2.3.3 NTM preemption versus stabilization

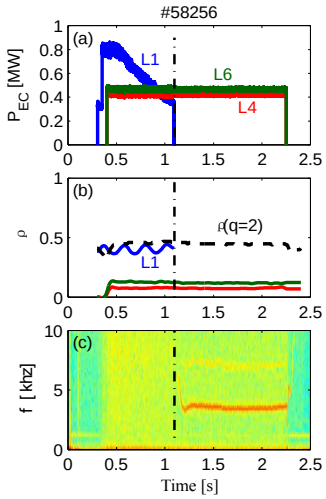

FIG. 8. (a) EC power trace, (b) EC deposition location and (c) magnetic spectrogram of the NTM preemption experiment (#58256)

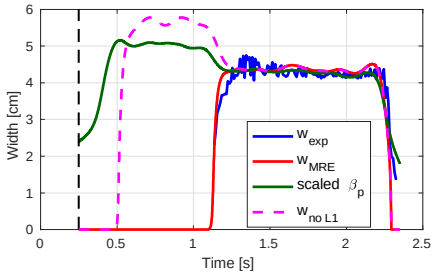

FIG. 9. Full island width evolution (#58256)

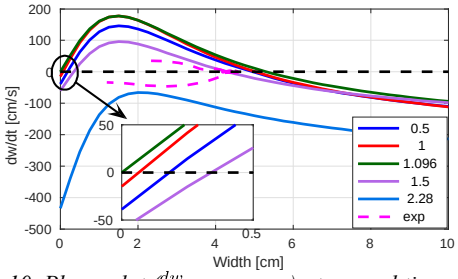

FIG. 10. Phase plot ($\frac{dw}{dt}$ $versus$ w) at several time slices

As a method of NTM control, the preemption of NTMs is explored as well. In principle this allows avoiding NTMs altogether and can be the preferred control method, but note that it penalizes the Q factor and may be prohibitive for some scenarios [2]. An example of NTM preemption is shown in Fig. 8, where $L1$ is switched on at $t = 0.3s$ and sinusoidally sweeps around the 2/1 rational surface, while L_4 and L_6 are turned on at $t = 0.4s$ and deposit near the plasma center with their full power. All these launchers are set to drive co-ECCD. A ramp down of $L1$ power is applied and no 2/1 NTMs are triggered until turning off $L1$ completely. This means that 2/1 NTMs are successfully preempted with only 0.36MW, while in a similar stabilization test ($L1$ is turned on after NTM triggering, with a ramp up of its power and similar sinusoidal sweeping around $q = 2$ as in #58256),

the mode cannot be fully stabilized with 0.75MW. This suggests a much higher efficiency of NTM preemption than stabilization, at least when sweeping is applied. However, preemption may require a much longer temporal duration of the EC power and thus a larger input energy, which needs to be taken into account in the trade-off.

Simulations with the MRE model are shown in Fig. 9, starting from $t = 0.25s$ with $w = 0$. The red curve fits very well both the timing of NTM onset and the saturated phase after triggering. Once again the same coefficients as in Table 1 have been used, except for a slightly different w_{de} ($1.9cm$ instead of $1.8cm$) and a_2 (2 instead of 2.1). The preemption effect results from the local effects of off-axis co-ECCD (with $\overline{\rho}_{mn}\Delta'_H \leq \overline{\rho}_{mn}\Delta'_{CD} < 0$) as well as the favourable curvature ($\overline{\rho}_{mn}\Delta'_{GGJ} < 0$) that all together counteracts the positive $\overline{\rho}_{mn}\Delta'$ that tends to trigger the mode. The phase plots at several time slices are shown in Fig. 10 and one can see that at $t = 1.096s$ (green), $\frac{dw}{dt}$ goes just above 0 at $w = 0$ and leads to the onset of the NTM. To have an idea of the preemption effect, another simulation (dashed magenta) is shown in Fig. 9, assuming no power from $L1$. In this case the mode would have been triggered at $t = 0.5s$, 100ms after turning on L_4 and L_6 power, similar to the NTM onsets presented before (#58477 and #56171).

3. REAL-TIME MULTI-ACTUATOR CONTROL

3.1 A generic task-based multi-actuator control framework

The reliable and efficient control of NTMs contributes to the design of a generic NTM controller that can be readily integrated in a plasma control system (PCS) that can simultaneously fulfill multiple control objectives with a limited set of actuators. This is especially crucial for complex experiments on long-pulse tokamaks. To this aim, a generic PCS architecture has been proposed, implemented and tested experimentally on TCV for the first time [14][15]. As shown in Fig. 11, in the new framework, the PCS is separated into an interface and a tokamak-agnostic layer. The interface layer translates tokamak-specific signals from actuators and diagnostics into generic ones to be used by the tokamak-agnostic layer, and vice versa. For example, a plasma and actuator state reconstruction block uses RT diagnostics as well as RT simulations to generate a generic continuous-valued representation of the state of both plasma and actuators. Specifically, RT analyses of magnetic perturbations have been used to provide estimations of mode type, amplitude and frequency [26], the RAPTOR observer [27] to reconstruct electron temperature and q profiles, the RAPDENS-observer [28] to estimate density profiles and RT-TORBEAM [29][30] to calculate EC beam depositions. This continuous-valued state is then translated by a generic plasma state monitor into a discrete finite-state representation of the conditions in plasma, with state transitions triggered on user-defined thresholds [15].

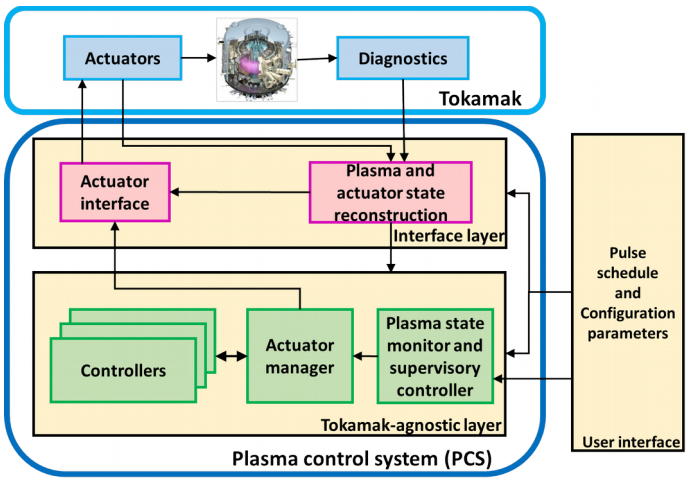

FIG. 11. Overview of the generic plasma control system framework [14][15].

In many present-day examples, control goals are achieved with tokamak-specific controllers, based on specific diagnostics and actuators. We propose an alternative task-based approach [14], wherein tokamak-agnostic controllers with standardized interfaces are used to carry out tasks using generic actuator resources. This allows a clear separation of the tokamak-agnostic layer from the tokamak-specific systems, and provides a layer of abstraction for operators as they only have to specify control tasks, without having to consider the functionality of each controller. Based on the defined tasks, the discrete state and the pulse schedule, a generic supervisory controller [15] prioritizes various tasks, activates relevant tasks/controllers, and communicates the parameters specific to each control task. A task-based actuator manager (AM) [14] is also implemented, which optimizes the actuator allocation for each task based on the plasma state, the actuator state and limits, the task priority and the resource requests per task from the controllers.

In this framework, it is important that controllers are generic as well and do not require knowledge of specific scenarios. For instance, the NTM controller should be able to perform its tasks knowing only the type of EC to use (i.e. co-ECCD), the m and n number of the mode to control, the presence, width and frequency of the mode, and possibly some standard plasma parameters like n_e and T_e that can be used to predict the mode evolution and compute in RT the required power for NTM control by solving the MRE inside the control system. This generic and versatile NTM controller is able to carry out all the NTM control experiments mentioned in Section 2.3 and has been included in the integrated control tests that will be discussed below.

3.2 Simultaneous RT control of β and NTMs on TCV

The generic PCS framework has been successfully implemented on TCV. Using a first version of the system, with generic controllers but lacking an AM, RT simultaneous control of NTMs, β and model-estimated q profiles has been achieved on TCV for the first time [10]-[13]. Recently, the full system with plasma state monitor, supervisory controller and AM has been tested for RT control of NTMs and β [14][15] and an example is shown in Fig. 12. In this test, two X2 EC launchers (L_4 and L_6) with a nominal power of 0.5MW each are used as the actuators and three control tasks are specified: central heating/co-ECCD, β control and NTM stabilization, as listed in Table 2. Task 1 is activated at the beginning of the discharge to establish the operational equilibrium. The β control task aims to track a reference value for β. The NTM stabilization task is activated and assigned the highest priority (i.e. 1) only if a mode is detected within its task activation window, otherwise β control takes the highest priority. As shown in Fig. 12(a) and (b), Task 1 is the only activated task during ①-② and is assigned priority one by the supervisory controller and both launchers by the AM. A 2/1 NTM is detected at ② and ⑥ respectively and NTM control task takes the highest priority until the mode is stabilized.

TABLE 2. List of control tasks

Task	Task Name	Task activation window, s	Power request, MW	Controller
1	Central heating/co-ECCD	[0.4 0.55]	[0 1]	NTM controller
2	NTM stabilization	[0.5 2.5]	[0 0.5]	
3	β control	[0.5 2.5]	[0 1]	Performance controller

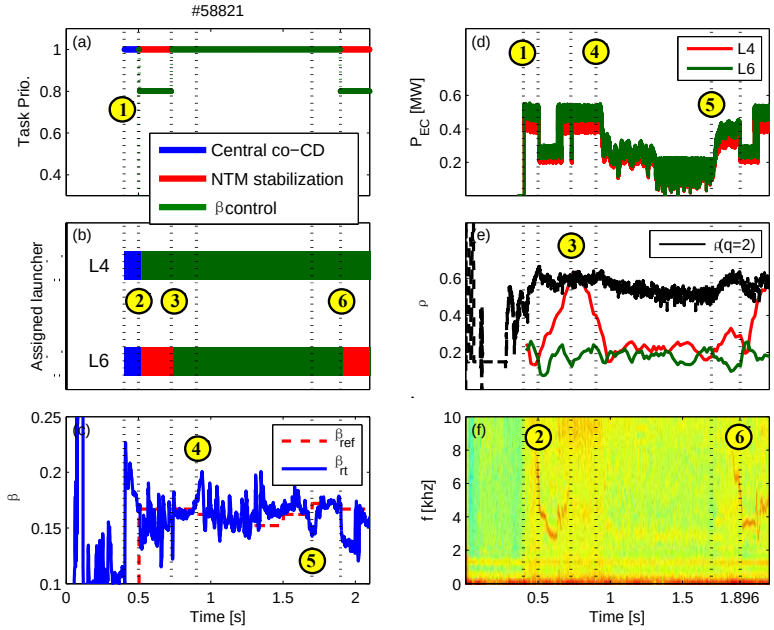

FIG. 12. Results of integrated control experiment with three control tasks and two EC actuators [14][15]. ① Central co-CD is activated; ②&⑥ NTM is detected; ③ NTM is stabilized; ④ lower β reference; ⑤ increase β referece.

The EC power and launcher deposition locations are shown in Fig. 12(d) and (e). During ①-②, maximum power as well as central deposition location of L_4 and L_6 are requested by Task 1. Upon the appearance of NTMs (② and ⑥), L_4 is assigned to Task 2 by the AM and is moved toward the mode location following the request of the NTM controller that is used to perform this task; a low power (about $0.23MW$) is requested during the movement of L_4 to minimize the perturbations to the plasma while full power ($0.5MW$) is asked once L_4 is close enough to the mode location to maximize the stabilization effect. Note that L_4 and L_6 share the same power cluster so they always convey the same power. It is worth mentioning that the NTM stabilization task is able to adjust its power request based on the timing of NTM stabilization, i.e. more power will be

requested if the mode still exists after the given power has been reached and a pre-set sweeping cycle around the mode location has been completed. This feature has been demonstrated in other tests [11][14] but is not shown here as $0.5MW$ is sufficient to fully stabilize the mode in this case. Once the mode is stabilized (③), L_4 is assigned to the β control task again by the AM and moved back to the center.

The β control result is shown in Fig. 12(c). With the presence of NTMs (②-③), the RT estimated β cannot reach its reference due to the degradation caused by NTMs and the lack of available power for this task. Without NTMs, the RT β matches the reference quite well, for example at ③-④ and ⑤-⑥; at ④, however, the β reference decreases, RT β oscillates and cannot follow the reference well because the EC power command reaches the actuator limits and cannot be lowered further; at ⑤, the β reference increases again, the power command increases as well and triggers a NTM at ⑥.

4. CONCLUSIONS

Various aspects concerning the control of 2/1 NTMs have been studied experimentally and numerically on TCV. It has been shown for the first time that the sinusoidal sweeping of co-ECCD beam around the rational surface is effective for both NTM stabilization and preemption. It is also shown that preemption is more than twice as efficient as stabilization in terms of the minimum power required, at least when sweeping is applied. A simple analytical model has been proposed to evaluate the time-varying Δ', which allows one to simulate very well the entire island width evolution, starting from zero width and including NTM preemption and stabilization, with very similar parameters. A generic PCS framework that is independent of the special features of TCV has been proposed and tested experimentally. Simultaneous control of NTMs and β has been demonstrated on TCV with generic RT plasma state reconstruction, monitoring, controllers, and advanced supervisory controller and AM.

ACKNOWLEDGEMENTS

This work has been carried out within the framework of the EUROfusion Consortium and has received funding from the Euratom research and training programme 2014-2018 under grant agreement No 633053. The views and opinions expressed herein do not necessarily reflect those of the European Commission.

REFERENCES

[1] SAUTER, O., BUTTERY, R.J., FELTON, R., et al., Plasma Phys. Control. Fusion 44 (2002) 1999-2019.
[2] SAUTER, O., HENDERSON, M.A., RAMPONI, G., et al., Plasma Phys. Control. Fusion 52 (2010) 025002 (17pp).
[3] LA HAYE, R.J., PRATER, R., BUTTERY, R.J., et al., Nucl. Fusion 46 (2006) 451-461.
[4] WESTERHOF, E., DE BLANK, H.J., PRATT, J., Nucl. Fusion 56 (2016) 036016 (6pp).
[5] FÉVRIER, O., MAGET, P., LÜTJEN, H., et al., Plasma Phys. Control. Fusion 58 (2016) 045015 (14pp).
[6] FELICI, F., GOODMAN, T.P., SAUTER, O., et al., Nucl. Fusion 52 (2012) 074001 (10pp).
[7] HUMPHREYS, D.A., FERRON, J.R., LA HAYE, R.J., et al., Phys. Plasmas 13 (2006) 056113 (13pp).
[8] PETTY, C.C., LA HAYE, R.J., LUCE, T.C., et al., Nucl. Fusion 47 (2007) 371-377.
[9] ISAYAMA, A., MATSUNGAGA, G., KOBAYASHI, T., et al, Nucl. Fusion 49 (2009) 055006 (9pp).
[10] MALJAARS, E., FELICI, F., BLANKEN, T.C.,et al., Nucl. Fusion 57 (2017) 126063 (19pp).
[11] KONG, M., et al., 44th EPS Conference on Plasma Physics, Belfast, the UK, (2017).
[12] VU, T., NOUAILLETAS, R., LEFEVRE, L., et al., Control Eng. Practice 54 (2016) 34-45.
[13] MAVKOV, B., WITRANT, E., PRIEUR, C., et al., Control Eng. Practice 60 (2017) 28-38.
[14] VU, T., BLANKEN, T.C., KONG, M., to be submitted to Nucl. Fusion (2018).
[15] BLANKEN, T.C., FELICI, F., GALPERTI, C., submitted to Nucl. Fusion (2018).
[16] SAUTER, O., LA HAYE, R.J., CHANG, Z., et al., Phys. Plasmas 4 (1997) 1654 (11pp).
[17] DE LAZZARI, D., WESTERHOF, E., Nucl. Fusion 49 (2009) 075002 (8pp).
[18] SAUTER, O., ANGIONI, C., LIN-LIU, Y.R., Phys. Plasmas 6 (1999) 2834-2839; Phys. Plasmas 9 (2002) 5140.
[19] FIZPATRICK, R., Phys. Plasmas 2 (1995) 825-838.
[20] REIMERDES, H., SAUTER, O., GOODMAN, T., et al., Physics Review Letters 88 (2002) 105005 (4pp).
[21] WHITE, R.B., MONTICELLO, D.A., ROSENBLUTH, M.N., et al., Phys. Fluids 20 (1997) 800-805.
[22] PLETZER, A., PERKINS, W., Phys. Plasmas 6 (1999) 1589-1600.
[23] KONG, M., et al., in preparation for Nucl. Fusion.
[24] PEREVERZEV, G., YUSHMANOV, P., Automate System for Transport Analysis, IPP 5 vol 98, Garching, 2002.
[25] MATSUDA, K., IEEE Trans. on Plasma Science 17(1989) 6-11.
[26] GALPERTI, C., CODA, S., DUVAL, B.P., et al., IEEE Trans. Nucl. Science 64 (2017) 1446-1454.
[27] FELICI, F., et al., 26th IAEA Fusion Energy Conference, Kyoto, Japan, 2016.
[28] BLANKEN, T.C, FELICI, F., RAPSON., C.J., et al., Fusion Eng. Design 126 (2018) 87-103.
[29] POLI, E., BOCK, A., LOCHBRUNNER, M., et al., Comp. Phys. Communications 225 (2018) 36-46.
[30] REICH, M., BILATO, R., MSZANOWSKI, U., et al., Fusion Eng. Design 100 (2015) 73-80.